Surface deformation in the region of the 1905 Kangra Mw=7.8 earthquake in the period 1846-2001

K. Wallace, R. Bilham and F. Blume
CIRES & Department of Geological Sciences, University of Colorado, Boulder, Colorado, USA

V.K. Gaur
Institute of Astrophysics, Bangalore, India

V. Gahalaut
National Geophysical Research Institute, Hyderabad, India

Abstract. One century after the Mw=7.8 Kangra earthquake of 4 April 1905, we report weak constraints on its rupture parameters based on the remeasurement of historic triangulation sites in the epicentral region. The along-arc length and down-dip width of the rupture were probably less than 100 km x 55 km, suggesting that further earthquakes are necessary to permit slip of the entire plate boundary. The geodetic data do not well constrain the slip, but a slip of ≈3.6 m is consistent with the rupture area. The Kangra earthquake may have incompletely released a 7 m slip deficit accumulated since a great earthquake in the 15th century. The Kangra rupture could fail again today in a Mw=7.5 earthquake (1.4 m of slip), or the surrounding ±150 km region could re-rupture the Kangra region as part of a much larger earthquake (>9 m of slip, Mw≈8.6).

1. Introduction

The Mw=7.8 Kangra earthquake was the most devastating Himalayan earthquake of the past 300 years, killing 20,000 people. For many years, the Kangra earthquake was considered to be a Mw=8.0 event, leading to the interpretation that the rupture spanned the entire width of the Himalayan plate boundary for a ≈300-km arc-parallel distance outlined by inferred Rossi-Forel isoseismal intensity VIII contours [Middlemiss, 1905; 1910, Seeber and Armbruster, 1984; Ni and Barazangi, 1984]. A re-evaluation of seismograms for the event, however, revealed that the magnitude was actually Ms=7.8 [Ambraseys and Bilham, 2001] and the area of its isoseimal contours had been exaggerated [Ambraseys and Douglas, 2004].

Following the 1905 earthquake, Burrard [1910] reported 15 cm of apparent uplift in the Dehra Dun region, and this supposed signal has been incorporated into a large number of studies. The leveling data, however, include substantial systematic errors indicating that vertical deformation was improbable [Bilham 2001]. Subsequent analysis of the revised MSK intensity data and the original seismograms suggest that the Kangra earthquake triggered a deep earthquake near Dehra Dun a few minutes after the mainshock, accounting for the high local intensities of MSK VIII at Mussoorie [Hough et al, 2005].

In 1846-1850 the Great Trigonometrical Survey of India (GTS) measured a series of triangles along the southern edge of the Himalaya [Walker, 1873]. This series was supplemented by a secondary triangulation northwards, but the secondary data have never been published in a publicly available format. Following the 1905 earthquake, Burrard [1906] re-measured triangles near Dehra Dun, 250 km from the epicenter, to identify potentially large cartographic errors associated with displacements of the primary triangulation, as had been observed in the epicentral region of the 1897 Shillong earthquake [Bilham and England, 2001]. Finding no detectable changes, he assumed that epicentral deformation near the mainshock was also negligible. No measurements of the triangles near Kangra were made after the earthquake, nor, to our knowledge, since then.

In 2001 we occupied 14 GTS points using GPS methods (Figure 1). We estimated angle changes and linear strains between sites, then removed the spatial strain-field anticipated from 151 years of interseismic strain at present-day rates to isolate the coseismic signal associated with the 1905 earthquake. The best rupture estimate approximates a 100 km x 55 km rupture with slip of ≈4m, coincident with the MSK Intensity VIII contour.

2. Data Collection and Processing

The GTS monuments (Figure 1) consist of bedrock marks, small platforms, and masonry pillars. Where stations had been obviously altered or reconstructed, we measured probable offset from the GTS site description and estimated resulting position uncertainty (Table 1).

The data were collected using Trimble 5700 GPS receivers with Zephyr Geodetic antennae. Data at each site were collected at 30 s intervals for 2-5 days. We used RAHO as a local base station. The data were analyzed using Bernese 4.2 GPS processing software with IGS sites IISC, IRKT, KIT3, POL2, LHAS as regional constraints.

The published GTS coordinates are referenced to the Everest Spheroid, a reference frame whose precise origin and orientation relative to the International Terrestrial Reference Frame (ITRF) are unknown [DeGraaff-Hunter, 1916]. To avoid errors introduced by a direct coordinate comparison, we compare both angles and line-lengths measured in 1846 and 2001.

Measured GTS angles are accurate to 4 ppm and baseline lengths to 10 ppm. However, sparse station recovery severely limits the number of angles available for direct comparison (Figure 1). For those that are available, the raw GTS angles [Walker, 1873] were corrected for spherical excess and used to calculate horizontal planar angles (Table 2) and station-separation distances; these data were then compared to angles calculated from the GPS position data.

Where contiguous GTS points were not recovered, we compared strain changes between remote points using a method described by Blume [1999] (Table 3). This method recovers local scale information from published GTS positions by approximating the unspecified origin of the Everest spheroid, using the local geoid as a constraint.

The effects of 150 years of interseismic strain accumulation must be removed to reveal the coseismic signal. With a convergence rate of 14±4 mm/yr in the Kangra region [Powers et al., 1998; Wesnousky et al., 1999; Banerjee and Bürgmann, 2001], 2.1±0.6 m of interseismic convergence centered NE of the epicenter contributes to the observed strain signal. We calculate this interseismic strain near the GTS points by assuming that it occurs on a shallow-dipping fault with a locking depth of 15 km underlying the southern Tibet. The calculated strain is small; the average adjustment required is less than 2 seconds of arc for angles and an average of 2 μstrain for baselines. Although the interseismic signal does not alter the final results, we used the corrected values for subsequent analyses.

Excessive co-seismic strains for lines involving SOLA, GUMB, BAGA suggest that these points have been relocated since 1850. These three sites and all angles associated

with them have been removed from the analysis, a regrettable loss as GUMB and SOLA are the two sites closest to the inferred epicenter.

3. Rupture Parameters

We compare the observed surface deformation to synthetic deformation calculated for a range of planar rupture parameters [Okada, 1985]. The models calculate strains and angle changes for different endpoint locations, strike, dip, length, down-dip width, depth, rake and slip. The fit between observed and calculated deformation is evaluated using the chi-squared statistic, which allows the stations to be weighted by their individual measurement uncertainties. The uncertainty is the sum of the 3D GPS solution uncertainty (Table 1), the uniform GTS uncertainty of 4 ppm for angles and 10 ppm for lines, and station location uncertainties due to modification or reconstruction of the GTS sites.

The initial models use no *a priori* constraints, allowing all parameters to vary over a wide range (±100 km location, ±100 km length, ±30° strike, 0-20 km depth, 0-70 km width, 0-15° dip) (Figure 2). We incremented reverse-slip from 0-15 m and strike-slip ±5 m with 0.1 resolution (Figure 2).

Unconstrained calculations reveal that the geodetic data are largely insensitive to rupture depth, dip and width, so we fixed these at 7°, 5 km and 55 km respectively. The selected dip and depth are consistent with a decollement determined from structural geology [Powers et al., 1998] and seismicity [Ni and Barazangi, 1984]. Our preferred solutions for the SW edge of the probable rupture suggest that its NE edge lies close to the line of microseismicity marking the transition from the locked interseismic zone beneath the Himalaya to inferred creep beneath the Tibetan plateau (Figure 1). Elsewhere this transition follows the 3.5 km elevation contour [Avouac, 2004]. Using this line as a NE constraint we examined model fits for a 100-300 m range of rupture length.

4. Results

Due to the sparseness of complete GTS triangles available for remeasurement, the angular data alone are unable to constrain fault slip, and favor a solution west of the known epicentral region. Disappointingly, slip anywhere between ±15 m provides

answers with $\chi^2 > 4$ and within 1σ of observed values. The explanation for this lack of constraint is that few triangles embrace any significant portion of the probable rupture (Figure 1). The best solution for the unconstrained linear strain also favors rupture significantly west and south of the maximum intensities epicentral region of the earthquake. By introducing reasonable geological and seismic constraints, however, the geodetic data can be used to quantify certain parameters of the rupture geometry.

The best-fitting solution corresponds to a 100-km-long fault with a strike between 140-158°, approximately underlying recently evaluated MSK VIII intensities and parallel to structural trends in the region. If the fault endpoint is fixed at 32.1° N, 76.2° E, the closest region of MSK VIII to the data, the optimal reverse slip is is 2.8 m with –0.7 m of strike-slip (Mw = 7.7). If the fault endpoint is shifted ≈30 km to 32.0°N, 76.0°E, permitted dip-slip grows to 7.5 m and strike-slip to 1.6 m (Mw = 8.0).

Rupture length is not well constrained. The best fitting fault rupture has length 100 km and strike 158° with 2.8-8 m of total oblique slip. The goodness-of-fit is poor ($\chi^2 >$ 10), but the variances of measurements are such that the best-fit result provides calculated strains that fall within one standard deviation of the observations.

By constraining the slip to the range of values found by the linear strain method, the sparse angle data can be used to better constrain the fault location, strike and length. The lower set of slip values (2.8 m dip-slip, -0.7 m strike-slip) results in a 60-km-long fault with a SW endpoint located at 32.36°N, 75.14°E, considerably north and west of the epicentral region. The higher range of slip values (7.5 m dip-slip, 1.6 m strike-slip) results in a fault 99 km long with a strike of 155° and an endpoint located at 31.8°N, 76.42°E. This rupture partially underlies the MSK Intensity VIII contour, though the correlation is not exact.

The possibility of the fault extending as far southeast as Dehra Dun is tested by varying the length from 200-300 km, and solving for its most appropriate location. The best-fit result requires a fault with an endpoint at 32.90°N, 75.14°N, a poorly constrained length >240 km and a tightly constrained strike of 159°; this rupture is implausible given the location of the epicentral region and known subsurface geology. The angular change data also do not support a very long rupture length.

5. Discussion and Conclusions

Although the distribution of surviving GTS stations near the Kangra 1905 rupture is sparse, changes in angles and line lengths in the past 150 years, combined with seismological and geological constraints, provide bounds on 1905 rupture location and area. The observed deformation is consistent with a NE dipping rupture with ~100 km length, 155°±5 strike, with its western corner located at 32.1°±0.1 N, 76.2°±0.2 E. Total reverse-slip lies in the range of 2-8 m, with left-lateral strike-slip motion between –1 and +2 m.

The preferred geodetic result approximates the area of the MSK Intensity VIII contour. If we use the instrumental magnitude of Ms=7.8 as a constraint on moment release and combine it with our preferred rupture area of 100 km x 55 km, we derive a probable mean slip of 3.6 m [Hanks and Kanamori, 1997]. Increasing the rupture length by 50%, reduces the slip accordingly, but would extend the rupture into the region of Intensity V and VI observations that are unlikely to overlay the mainshock rupture.

The SW edge of the inferred 1905 rupture (Figure 1, shaded) corresponds to the Jawalamucki Thrust fault [Powers et al. 2002], although no surface slip was reported on this fault in 1905. The NE edge corresponds to the inferred geodetic locking line beneath the Greater Himalaya.

No significant earthquakes are recorded historically in the Kangra region prior to the 1905 event [Bilham, 2004], and the only known earthquake that may have ruptured the region is the one that caused surface slip on the Himalayan frontal thrusts c.1400 [Kumar et al., 2001; Wesnousky et al., 1999]. If we assume a steady convergence rate in this part of the Himalaya of 14-19 mm/yr (15±2 mm/yr, Banerjee and Bürgmann [2002]); 18.8±3 mm/yr, Jade et al., [2004]) the Kangra earthquake occurred at a time when a 7-9 m slip deficit had developed. The earthquake could have released most of this slip deficit, or as little as half of it. Displacements since 1905 have increased this slip deficit by 1.4-1.8 m.

Rupture areas of historical earthquakes in the regions to the east and west of Kangra are not well defined, but it is possible that no slip has occurred there since c.1400, resulting in a 9-11 m slip deficit. If the 1803 earthquake ruptured as far west as Kangra, the slip deficit may have been reduced; however, it is probable that the westernmost end of the 1803 rupture did not extend beyond 79°, or 200 km west of the Kangra rupture

[Ambraseys and Douglas, 2004]. A Kashmir earthquake in 1555 may have approached the Kangra region from the west, but this would still allow a 7.5-8 m slip deficit to have developed west of Kangra.

We conclude that the Kangra region currently has a slip deficit of at least 1.4 m, and probably more than 5 m if slip in 1905 was as little as 4 m. The region lies within a 300 km segment of the Himalayan plate boundary that has an inferred slip deficit of 7.5-9 m, and is surrounded both to the SW, NW and SE by regions of large slip deficit. If the Kangra 1905 region were to rupture now it could host a Mw=7.5 earthquake, or it could rupture as part of a larger earthquake (Mw≥8.5) extending >300 km along strike with a possible average slip of 9-11 m.

Acknowledgments. Funding for the investigation was provided by NSF grant EAR 0000359.

References

Ambraseys, N. and Bilham, R. (2000) A note on the Kangra Ms=7.8 earthquake of 4 April 1905, *Curr. Sci.*, *79:1*, 45-50.

Ambraseys, N. (2000) Reappraisal of north-Indian earthquakes at the turn of the 20th century, *Curr. Sci.*, *79:9*, 1237-1250.

Ambraseys, N. N. and J. Douglas, Magnitude calibration of North Indian earthquakes, *Geophys. J. Int.* (2004) 158, 1-42.

Bilham, R. (2001) Slow tilt reversal of the Lesser Himalaya between 1862 and 1992 at 78°E, and bounds to the southeast rupture of the 1905 Kangra earthquake, *Geophys. J. Int., 144*, 713-728.

Blume , Frederick. (1999) *Determination of source parameters of the great 1934 Nepal earthquake using historic and modern geodesy.* Ph.D. thesis, University of Colorado, Boulder, CO.

Burrard, S.G. (1906) Geodesy, in *Annual Report Board of Scientific Advice for India for the Year 1904-5,* pp. 42-52, Government Central Press, Calcutta.

Burrard, S.G. (1909) *Account of the Operations of the Great Trigonometrical Survey of India*, North East Longitudinal Series, Synoptical Volume XXXVB, Survey of India, Dehra Dun.

Burrard, S.G. (1910a) *Account of the Operations of the Great Trigonometrical Survey of India,* Descriptions of Heights of Bench Marks of the Northern Lines of Leveling, XIX, Survey of India, Dehra Dun.

Burrard, S.G. (1910b) Memorandum of the steps taken in 1905-10 to enable movements of the Earth's crust to be detected, in *Account of the Operations of the Great Trigonometrical Survey of India,* Appendix No. 3, Descriptions of Heights of Bench Marks of the Northern Lines of Levelling, XIX, Survey of India, Dehra Dun.

Hanks, T. C. & H. Kanamori (1997): A moment magnitude scale, J. Geophys. Res., 84, 2348-2350.

Hennesey, J.B.N. (1875) *Account of the operations of the Great Trigonometrical Survey of India*, Principal Triangulation of the Great Arc Meridional Series, V, Survey of India, Calcutta.

Hough, S.E., Bilham, R., Ambraseys, N., Feldl, N. (2004) Revisiting the 1897 Shillong and 1905 Kangra earthquakes in northern India: Site response, Moho reflections, and a triggered earthquake, *in preparation.*

Jade, S., Bhatt, B.C., Yang, Z., Bendick, R., Gaur, V.K., Molnar, P., Anand, M.B., Kumar, D. (2004) GPS Measurements from the Ladakh Himalaya, India: Preliminary tests of plate-like or continuous deformation. *GSA Bull.*, 116(11/12), 1385-1391.

Kumar, S., Wesnousky, S.G., Rockwell, T.K., Ragona, D., Thakur, V.C., Seitz, G.G. (2001) Earthquake Recurrence and Rupture Dynamics of Himalayan Front Thrust, India, *Science, 294*, 2328-2331.

Middlemiss, C.S. (1905) Preliminary account of the Kangra Earthquake of 4th April 1905, *Records geol. Soc. India, 32,* 258-294.

Middlemiss, C.S. (1910) The Kangra Earthquake of 4th April 1905, *Mem. Geol. Survey of India, 38*.

Okada. Y. (1985) Surface deformation due to shear and tensile faults in a half-space, *Bull. Seis. Soc. Amer.*, *75*, 1135-1154.

Powers, P.M., Lillie, R.J., Yeats, R.S. (1998) Structure and shortening of the Kangra and Dehra Dun reentrants, Sub-Himalaya, India, *GSA Bull.*, *110:8*, 1010-1027.

Seeber, L. and Armbruster, J.G. (1981) Great detachment earthquakes along the Himalayan arc and long-term forecasting, in *Earthquake Prediction: An International Review*, D.W. Simpson and P.G. Richards, eds., Maurice Ewing Series 4, Amer. Geophys. U.

Walker, J.T. (1873) *Account of the Operations of the Great Trigonometral Survey of India*, Principal Triangulation III, 1873, Survey of India, Calcutta.

Wesnousky, S.G., Kumar, S., Mohindra, R., Thakur, V.C. (1999) Uplift and convergence along the Himalayan Frontal Thrust of India. *Tectonics, 18:6*, 967-976.

Figure 1. Triangulation near the Kangra earthquake. Filled triangles indicate recovered GTS points, shaded large triangles were used in shear strain analysis, and bold lines indicate those used in linear strain analysis. Numbers in white boxes are the station numbers as listed in Table 1. The preferred rupture area is shaded. The MSK VIII contour is interpolated from Ambraseys and Douglas [2004], with observations indicated by MSK number. Closed circles indicate M>5.5 earthquakes since 1960; open circles indicate trench locations that define the 1400 rupture [Kumar et al, 2005].

Figure 2. Contours of the calculate χ^2 statistic used for finding the best-fit parameter values. Despite the poor fits for all parameters, minima can be identified. a) Latitude and longitude. b) Slip. c) Strike and length. d) Strike and longitude (the best-fit latitude values varied little). Also shown is the contour for 1-σ of each calculation (thick line), with the exception of the slip plot, for which all reasonable values fall within the range of 1-σ.

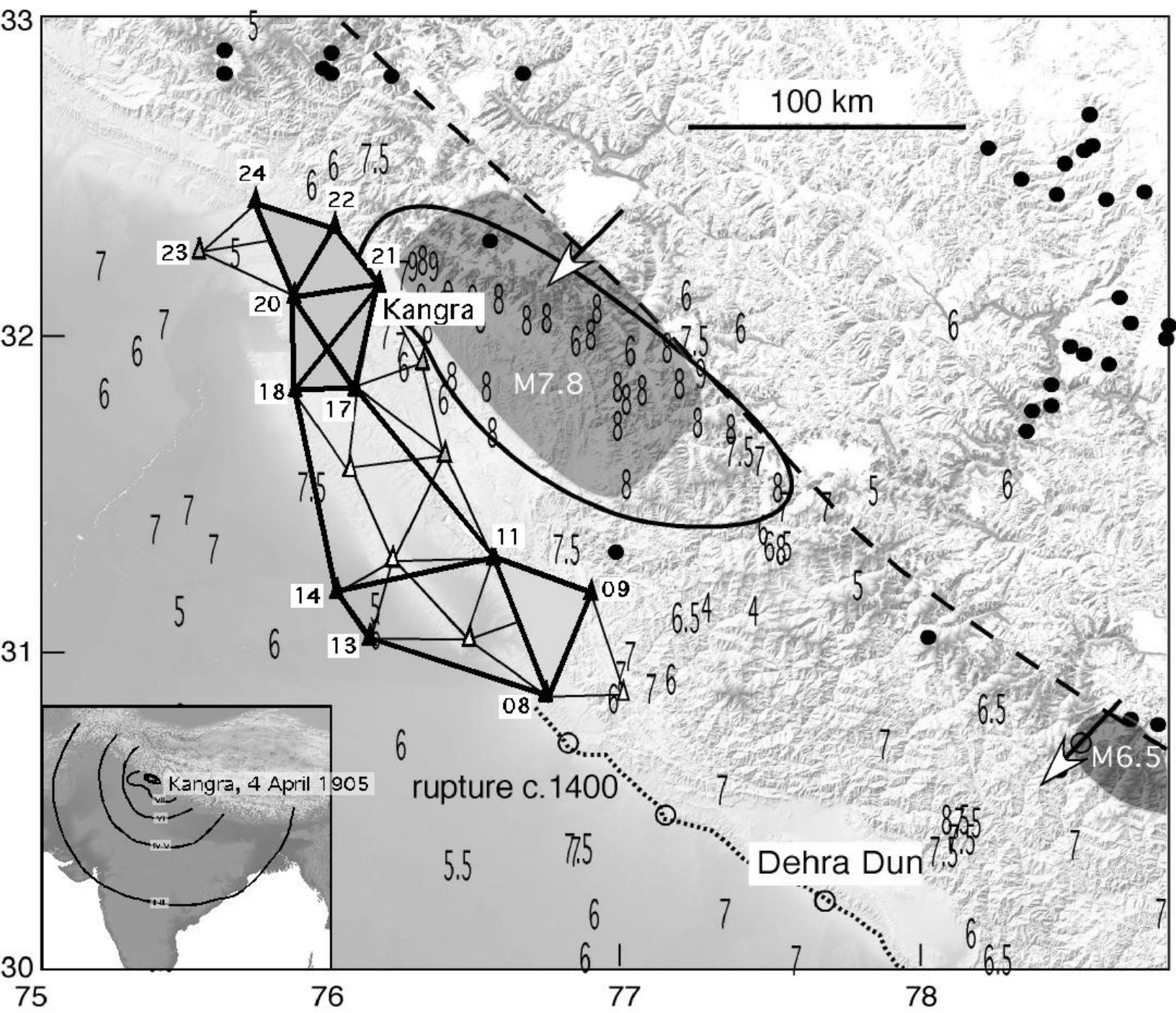
100 km
Kangra
M7.8
M6.5
rupture c.1400
Dehra Dun
Kangra, 4 April 1905
24
22
23
21
20
18
17
11
14
09
13
08
33
32
31
30
75
76
77
78

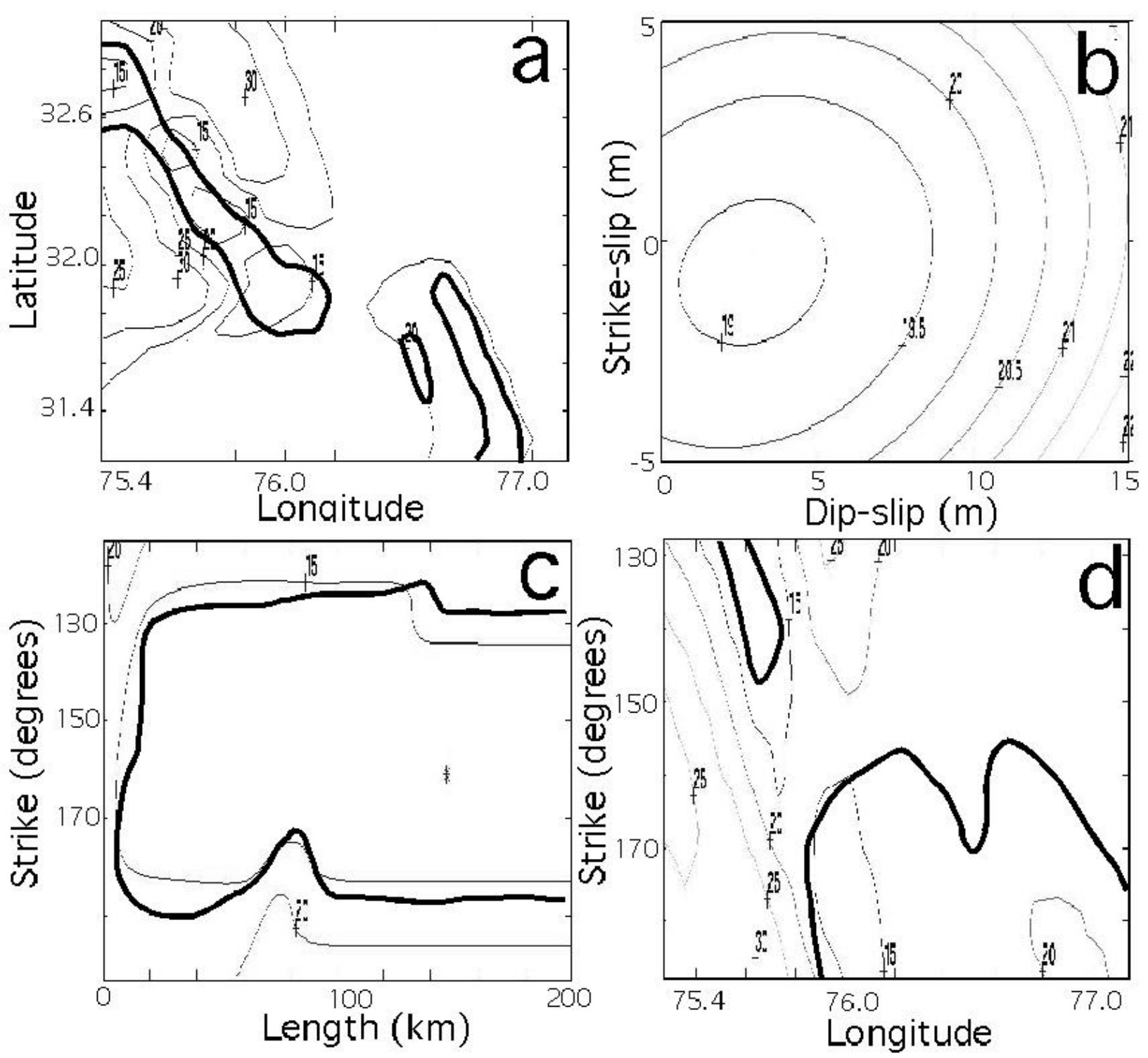
a
32.6
32.0
31.4
Latitude
75.4
76.0
77.0
Longitude
b
5
0
-5
Strike-slip (m)
0
5
10
15
Dip-slip (m)
c
130
150
170
Strike (degrees)
0
100
200
Length (km)
d
130
150
170
Strike (degrees)
75.4
76.0
77.0
Longitude

Table 1. GPS Station coordinates, uncertainties, and corrections applied to rebuilt or damaged GTS monuments.

Coordinates				Total Uncertainties		
GPS Site	**Long.**	**Lat.**	**Ht. (m)**	**Long. (m)**	**Lat. (m)**	**Ht. (m)**
23 BAGA	75.5236	32.2561	244.87	0.008	0.005	0.015
09 BARA	76.8851	31.1933	2029.60	0.010	0.004	0.016
24 DALA	75.7546	32.4304	802.13	0.012	0.008	0.021
20 DINA	75.8481	32.1306	585.30	0.011	0.007	0.020
08 GOCH	76.7175	30.8909	434.75	0.014	0.011	0.021
19 GUMB	76.2979	31.9211	1092.63	0.013	0.010	0.024
22 HATI	76.0057	32.3530	1558.50	0.013	0.008	0.022
14 HEON	75.9871	31.2084	222.07	0.009	0.004	0.016
18 KOTI	75.8473	31.8390	619.41	0.012	0.006	0.027
21 LIPI	76.1537	32.1480	845.82	0.009	0.007	0.016
11 NINA	76.5362	31.3059	1145.49	0.008	0.004	0.018
13 RAHO	76.1216	31.0531	233.35	0.004	0.002	0.007
16 SOLA	76.3808	31.6213	1103.45	0.008	0.008	0.009
17 TIPR	76.0694	31.8412	972.11	0.011	0.009	0.017

Table 2. Angular changes, observed and corrected for interseismic strain.

Triangle	Angle (rad)	Corrected (rad)	Change (mrad)	Uncertainty (mrad)
08 09 11	0.8033	0.8033	2.30	0.0114
09 08 11	1.4858	1.4858	-17.10	0.0399
11 08 09	0.8525	0.8525	14.80	0.0186
17 20 21	0.8062	0.8063	6.60	0.0098
20 17 21	1.0605	1.0605	7.10	0.0195
21 17 20	1.2749	1.2749	-13.70	0.0309
17 18 20	1.0046	1.0046	6.90	0.0089
18 17 20	1.5560	1.5560	-13.10	0.0231
20 17 18	0.5810	0.5811	6.20	0.0137
20 21 22	0.9613	0.9613	-12.10	0.0161
22 20 21	1.0938	1.0938	4.90	0.0089
20 22 24	0.7998	0.7998	0.70	0.0451
21 20 24	0.7619	0.7619	3.10	0.0180
24 20 21	0.6186	0.6186	8.30	0.0177
21 22 24	0.3246	0.3246	4.10	0.0451
24 21 22	0.3452	0.3452	2.50	0.0211

Table 3. Linear strains, observed and corrected for interseismic strain.

Baseline		L (km)	Azimuth	Observed	Corrected
24	22	25.15	110.01	-45.07	-47.17
24	20	34.40	165.26	-6.82	-4.89
22	20	28.81	210.90	-37.65	-38.42
22	21	26.68	148.63	-11.60	-13.07
20	21	28.90	86.08	-53.40	-50.77
20	18	32.33	180.15	19.11	14.88
21	18	44.87	219.99	6.36	4.91
21	17	34.95	193.15	-26.87	-26.44
18	17	21.03	89.29	95.29	92.93
18	14	71.18	169.26	-29.61	-30.13
17	14	70.61	186.35	-20.30	-21.96
17	11	74.08	143.27	-24.72	-24.97
14	13	21.47	143.39	53.88	53.87
14	11	53.42	78.12	-32.47	-41.90
11	13	48.46	210.89	-37.43	-38.51
11	09	35.53	110.59	-11.43	-11.93
13	08	59.70	107.46	-57.22	-57.30
09	08	37.19	205.44	-2.08	-4.57
08	11	49.17	159.44	-14.91	-15.31